International Journal of Geo-Information

MDPI

Article

Integration of Geostatistical and Sentinal-2AMultispectral Satellite Image Analysis for Predicting Soil Fertility Condition in Drylands

Mohamed S. Shokr [1,*], Yasser S. A. Mazrou [2,3], Mostafa A. Abdellatif [4], Ahmed A. El Baroudy [1], Esawy K. Mahmoud [1], Ahmed M. Saleh [4], Abdelaziz A. Belal [4] and Zheli Ding [5]

1 Soil and Water Department, Faculty of Agriculture, Tanta University, Tanta 31527, Egypt; drbaroudy@agr.tanta.edu.eg (A.A.E.B.); esawy.rezk@agr.tanta.edu.eg (E.K.M.)
2 Applied College-Muhyle, King Khalid University, Abha 62587, Saudi Arabia; ymazrou@kku.edu
3 Department of Agriculture Economic, Faculty of Agriculture, Tanta University, Tanta 31527, Egypt
4 National Authority for Remote Sensing and Space Science (NARSS), Cairo 11843, Egypt; mostafa.abdou@narss.sci.eg (M.A.A.); a.saleh@narss.sci.eg (A.M.S.); abelal@narss.sci.eg (A.A.B.)
5 Haikou Experimental Station, Chinese Academy of Tropical Agricultural Sciences, Haikou 571101, China; dingzheli@zju.edu.cn
* Correspondence: mohamed_shokr@agr.tanta.edu.eg

Abstract: For modelling and predicting soil indicators to be fully operational and facilitate decision-making at any spatial level, there is a requirement for precise spatially referenced soil information to be available as input data. This paper focuses on showing the capacity of Sentinal-2A(S2A) multispectral imaging to predict soil properties and provide geostatistical analysis (ordinary kriging) for mapping dry land soil fertility conditions (SOCs). Conditioned Latin hypercube sampling was used to select the representative sampling sites within the study area. To achieve the objectives of this work, 48 surface soil samples were collected from the western part of Matrouh Governorate, Egypt, and pH, soil organic matter (SOM), available nitrogen (N), phosphorus (P), and potassium (K) levels were analyzed. Multilinear regression (MLR) was used to model the relationship between image reflectance and laboratory analysis (of pH, SOM, N, P, and K in the soil), followed by mapping the predicted outputs using ordinary kriging. Model fitting was achieved by removing variables according to the confidence level (95%).Around 30% of the samples were randomly selected to verify the validity of the results. The randomly selected samples helped express the variety of the soil characteristics from the investigated area. The predicted values of pH, SOM, N, P, and K performed well, with R^2 values of 0.6, 0.7, 0.55, 0.6, and 0.92 achieved for pH, SOM, N, P, and K, respectively. The results from the ArcGIS model builder indicated a descending fertility order within the study area of: 70% low fertility, 22% moderate fertility, 3% very low fertility, and 5% reference terms. This work evidence that which can be predicted from S2A images and provides a reference for soil fertility monitoring in drylands. Additionally, this model can be easily applied to environmental conditions similar to those of the studied area.

Keywords: soil fertility modelling; GIS; ordinary kriging; cLHS; S2A image; drylands

Citation: Shokr, M.S.; Mazrou, Y.S.A.; Abdellatif, M.A.; El Baroudy, A.A.; Mahmoud, E.K.; Saleh, A.M.; Belal, A.A.; Ding, Z. Integration of Geostatistical and Sentinal-2AMultispectral Satellite Image Analysis for Predicting Soil Fertility Condition in Drylands. *ISPRS Int. J. Geo-Inf.* **2022**, *11*, 353. https://doi.org/10.3390/ijgi11060353

Academic Editors: Dimitris Triantakonstantis, Panagiotis Tziachris and Wolfgang Kainz

Received: 11 April 2022
Accepted: 14 June 2022
Published: 17 June 2022

1. Introduction

Soils are very complicated ecosystems formed by biological and non-biological factors that widely fluctuate from one environment to another. Applying suitable agricultural management practices requires the characterization, modelling, and mapping of soil properties [1–4]. Models of soil properties and indicators require the use of accurate, spatially referenced soil information as an input to help facilitate the decisions made at national and international levels [5]. Estimating different soil properties by traditional methods requires intensive field and laboratory work; this is time-consuming, costly, and the results may

also be affected by significant uncertainty [6]. Thus, the combination of remote sensing data and field measurements has been proposed as a way to model and map soil properties [7,8]. Furthermore, increasingly high-quality data, including digital elevation models (DEMs) and satellite images, have allowed for novel methods to be established to select the samples distributed within the feature space of environmental variables. Conditioned Latin hypercube sampling (cLHS) is an atypical example [9]. It has been implemented in many mapping studies in terms of guaranteeing the full coverage of a multivariate feature space [10–23]. Some critical soil properties, such as salinity, texture, minerals, and organic matter, have been estimated and investigated using enhanced thematic mapper plus (ETM+), Landsat-7, and Landsat-8 operational land imagers (OLIs) [24]. Visible, near-infrared, and short-wave infrared hyper spectral methods have been used to estimate surface soil properties such as soil organic carbon (SOC), cation exchange capacity, soil texture, and calcium carbonate [25–29]. One of the major challenges today is finding the best way to develop low-cost methods for modelling and mapping physical and chemical soil properties over large areas. Remote sensing (RS) has commonly been utilized, mainly at a regional scale, for soil mapping because of the low costs, quick data acquisition, and availability of high temporal and spatial information quality [30]. Satellites and aerial platforms that are used for capturing bare soil images can be analyzed by traditional methods, such as band ratio and discriminant analysis [30]. An adequate prediction of soil properties using hyperspectral data is not easy due to the soil reflectance phenomenon. To overcome this problem, regression analysis, including multiple regression analysis (MLR), principal component regression (PCR), and partial least-squares (PLS) regression, have been used, with these making connections between soil properties and reflectance data or spectral indices [30,31]. The use of hyperspectral VNIR/SWIR imagery was confirmed by a previous study as being a very important tool for mapping soil properties, however, it cannot be implemented for large areas or for long time periods due to high cost and low availability [5]. The low temporal resolution of VNIR/SWIR multispectral, coarse spatial, and spectral resolutions within these sensors causes deficiencies in spatial prediction performance under the annual crop system, as the time period of bare soil availability is very short [32,33]. The European Space Agency launched multispectral satellite Sentinal-2A data last November (2015), with its development of large area images considered revolutionary [5]. Sentinal-2A (S2A) data was released last November (2015); it contains high temporal, spatial (10 to 60 m), and spectral resolutions (20 to 180 nm) [5,33]. Today, to identify elements that are deficient in a soil, there is a requirement for quick analysis with low cost and high accuracy; satellite image data can complement analysis in situ [34,35]. Precise measurements and efficient methods should be conducted to improve soil and water quality [36]. Measurable information for soil characteristics and their spatial spreading is very important to achieve agriculture sustainability development and reduce negative environmental effects [37–39]. This is very critical in drylands due to these areas having a lot of limiting factors for soil fertility, such as a low content of nitrogen (N), phosphorus (P), potassium(K), soil organic matter (SOM %), and irrigation water scarcity. The mapping of these factors provides a good indicator of land degradation [40–42]. Recently, the development of low-cost approaches is needed for mapping soil properties within a large area. Additionally, it is critical to consider that the management of agricultural lands require a method of rapid analysis to characterize the elements deficient in soil and in crops as well. Therefore, this research aims to assess the potential of S2A imaging and geostatistical analysis (ordinary kriging) to predict selected soil properties and show the distributions of fertile conditions of study area based on the predicted properties. The study areas focus on western parts of Matrouh Governorate (Northwest coast of Egypt), parts of which were used previously as test areas for mapping using Vis-NIR Spectroscopy data. The proposed approach enabled us to model relationships between the spectral reflectance, which was extracted from bands of S2A satellite imagery, and laboratory analysis, to create maps of soil properties by using OK and finally produce of SOC maps.

2. Materials and Methods

The proposed procedure in this work is displayed in Figure 1.

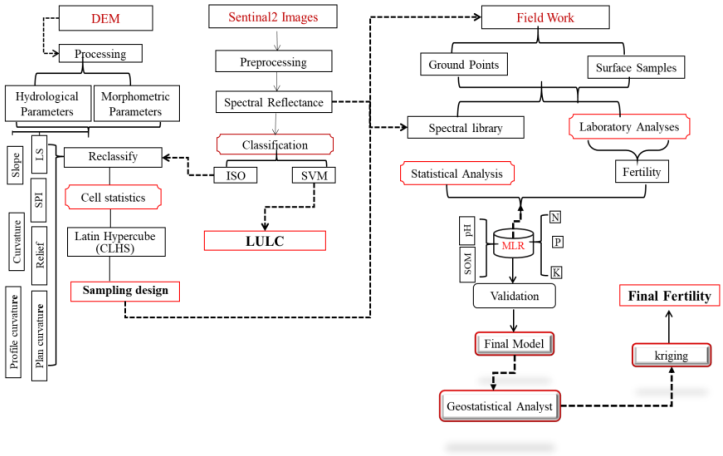

Figure 1. Schematic diagram of current work methodology; note: MLR = multi linear regression.

2.1. Study Area

The experimental area is located in the western part of Matrouh Governorate, Egypt, between longitudes 26°49′58.0″ and 26°58′06″ East, and latitudes 31°13′07″ and 31°26′36″ North with a total area of 213.7 km^2 (Figure 2). The study area has a wide variety of environmental conditions [43,44] and is characterized by a Mediterranean Sea climate, with rainfall fluctuating between 105 and 200 mm per day and the mean temperatures of 8.1 to 18 °C and 20 to 29.2 °C in the winter and summer seasons, respectively [6]. The area suffers from low-density vegetation cover during the summer, with the vegetation cover starting to increase in the winter and spring due to precipitation. The land elevation differs between 11 and 212 m above sea level (asl), as can be seen in Figure 3, with the lowest areas located closest to the Mediterranean Sea and the highest areas appearing in the southern region (Figure 3) [6]. Miocene and Quaternary deposits are the main geological units [44,45]. The main geomorphologic units in the study area are plains (3453.68 ha), wadi (733 ha), terraces (7149.65 ha), basins (399.27 ha), pavement plain, and reference unit (11,064.76 ha) units, according to [46]. Figure 4 shows the three classes of land use and land cover (LULC) highlighted in the investigated area: agriculture, urban, and bare soils. These classes cover 1064.26 (5%), 273.36 (1.3), and 20,210.76 (93.7%) hectares (ha) of the study area, respectively. The soils of the study area are classified into two orders, i.e., Entisols and Aridisols, which are divided into five subgroups: *Typic TorriPsamments*, *Typic Calcigypsids*, *TypicHaplogypsids*, *Typic Haplocalcids* and *Lithic Torriorthents* [44,47].

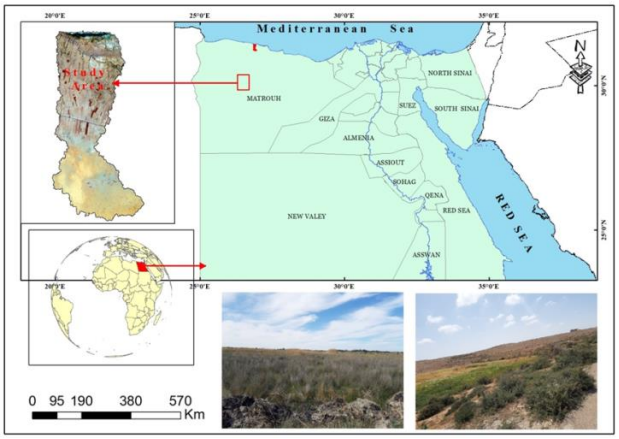

Figure 2. Location of the investigated area.

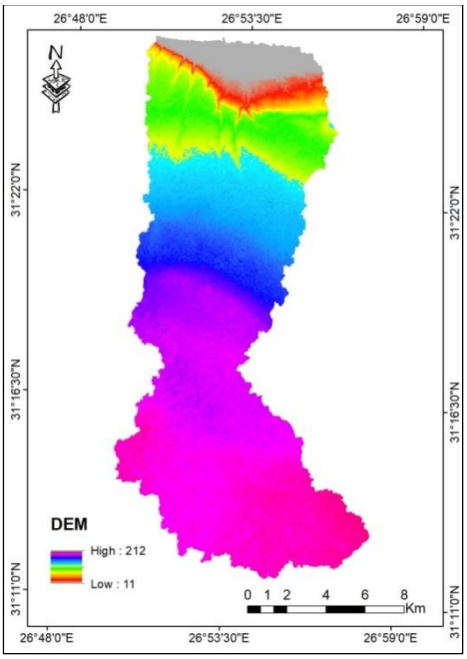

Figure 3. Digital elevation model (DEM) of the investigated area.

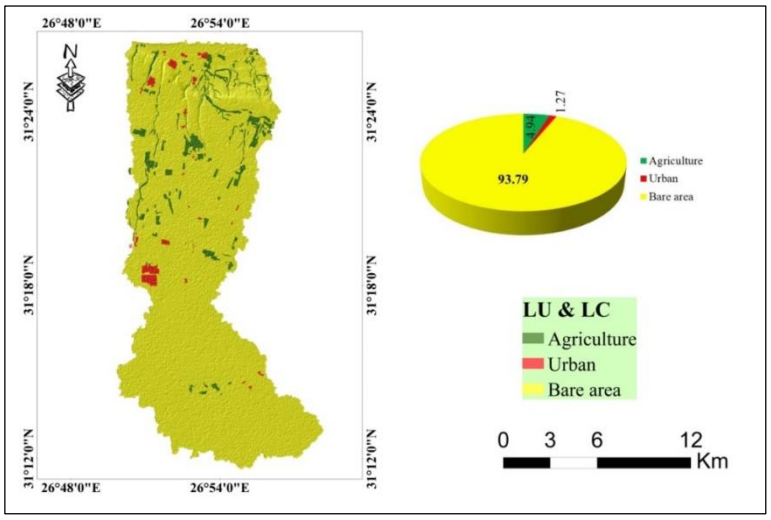

Figure 4. Land use (LU) and land cover (LC) of the study area.

2.2. Soil Sampling and Laboratory Analysis

Conditioned Latin hypercube sampling (cLHS) was utilized to realize the best sampling site distributions based on landscape attributes [9,48]. The sample points number was set at 400, and the iteration number was set at 50,000 as seen in Figures 1 and 5.The selection of the samples (400 points) was based on hydrological and morphometric parameters, i.e., digital elevation model (DEM), slope, curvature, profile curvature, plan curvature, stream power index, slope length, and ISO data classification of the S2A images (Supplementary Materials: Figures S1 and S2) [49], and urban areas were excluded. All soil sample locations were checked in the field; forty-eight locations were chosen to represent different landforms of the study area according to [46] (Figure 6). The soil samples were collected from the study area and transferred to the relevant soil, water, and plant laboratories within the Faculty of Agriculture, Tanta University in accordance with ISO/IEC 17,025:2017 requirements for analysis. The samples were air-dried under normal temperature and then passed through a 2 mm sieve. The soil organic matter proportion (SOM %) was analyzed according to the Walkley and Black method, while soil reaction (pH) was measured using

pH meter (V HANNA) [44]. The available nitrogen (N), phosphorus (P) and potassium (K) levels were determined by Kjeldahl spectrophotometry (880 wavelength) and flame photometry [50].

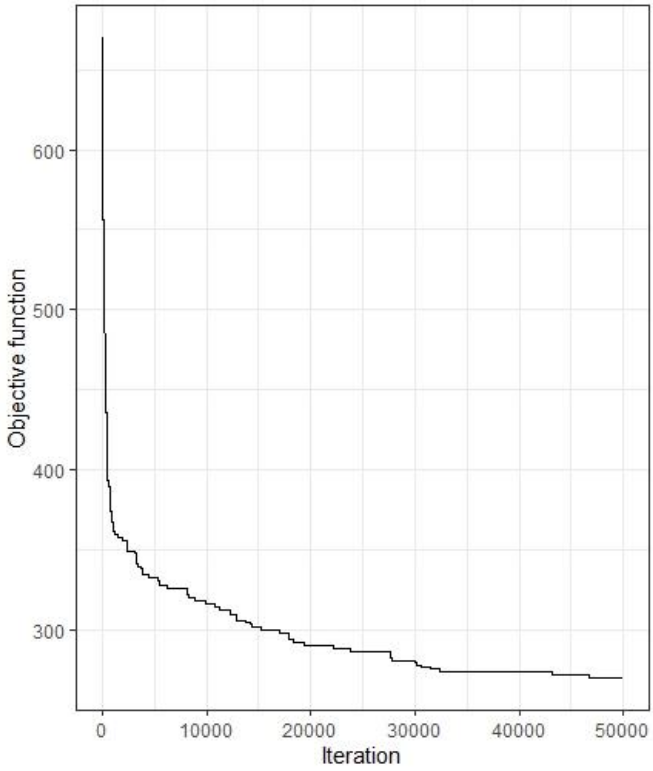

Figure 5. Iteration of selected parameters for CLHs.

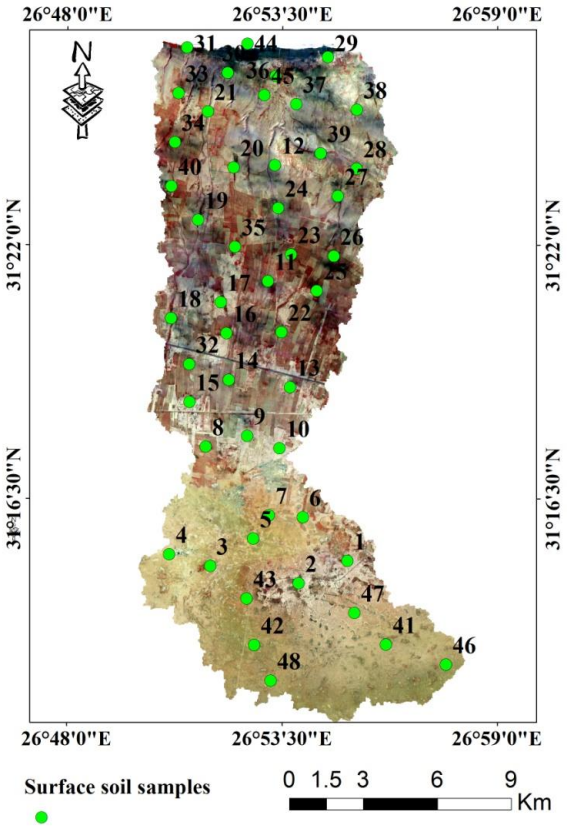

Figure 6. Distribution of surface soil samples within the study area.

2.3. Digital Image Processing

A Sentinal-2A image was acquired in the September of 2021, and low-density cloud data was downloaded from the United States Geological Survey (USGS). The multispectral S2A image has 13 spectral bands; four of them have10 m resolution, and six of the bands have a 20 m resolution (Table 1). The image was atmospherically corrected utilizing the ATCOR2 radiative transfer model according to [51]. Universal Transverse Mercator (UTM) coordinates were used for the geo-rectifying of the image. Then, all satellite image analyses and processes were carried out using the standard producers provided by SNAP software [52]. All spectral bands were resampled to 10 m by the S2A resampling function in the SNAP software (Figure 7).

Table 1. Characteristics of the Sentenial2 satellite image.

No.	Band Name	Central Wavelength (nm)	Resolution (m)
1	Coastal aerosol	443.9	60
2	Blue	496.6	10
3	Green	560	10
4	Red	664.5	10
5	Vegetation Red Edge	703.9	20
6	Vegetation Red Edge	740.2	20
7	Vegetation Red Edge	782.5	20
8	NIR	835.1	10
8a	Narrow NIR	864.8	20
9	Water vapour	945	60
10	SWIR–Cirrus	1373.5	60
11	SWIR	1613.7	20
12	SWIR	2202.4	20

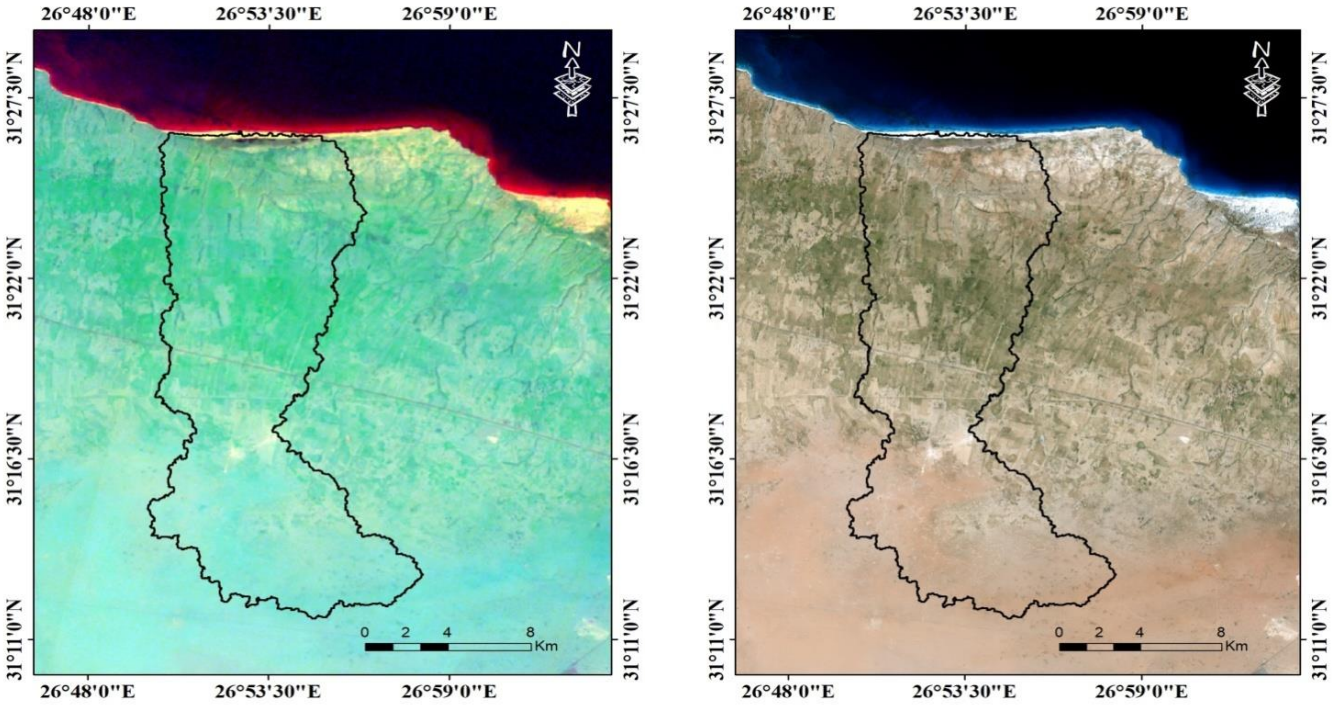

(**a**) (**b**)

Figure 7. Image resolutions within the study area: (**a**) 60 m and (**b**) the resampled image with 10 m resolution.

2.4. Procedure of Modelling

Multiple linear regressions (MLRs) were used to predict the dependent variable response, from the many independent variables, as a correlation function between them. The MLR algorithm was implemented using the SPSS V22, with stepwise (backward) analysis, fitting the model via the removal of variables according to the confidence level (95%). Around 70% of samples were used for calibration and 30% for validation. The average of the spectral reflectance from the S2A image was used to determine soil fertility parameters, i.e., pH, SOM, N, P, and K. The output maps were validated by calculating the correlation coefficient (R^2) and the root mean square error (RMSE) (Equations (1) and (2)). In addition, R^2 was utilized to also describe the validation of the model, where x expresses the value of the soil parameter i, which was analyzed in the laboratory and used as the background value for the calibration process. y represents the predicted value and n is the number of soil samples utilized for the calibration [53,54].

$$R^2 = 1 - \frac{\sum_{i=1}^{n}(y_i - \hat{y}_i)^2}{\sum_{i=1}^{n}(y_i - \overline{y_i})^2} \quad (1)$$

where n = the number of samples, y_i = measured value; $\hat{y}_i$ = the predicted value, and $\overline{y_i}$ = the mean ofallvalues.

$$\text{RMSE} = \sqrt{\frac{1}{N}\sum_{I=1}^{N}[Z_1(x_i) - Z_2(x_i)]^2} \quad (2)$$

where $Z_1(x_i)$ = measured values and $Z_2(x_i)$ = predicted values.

2.5. Producing Maps of Soil Properties

The prediction of soil property values was carried out using ordinary kriging (OK). OK is a geostatistical model that predicts selected soil properties in anon sampled location [55,56]. The histogram tool and normal QQ plots were used to check the normal distribution of data for each parameter. In this work, we implemented semi variogram models (Gaussian, spherical, and stable) for each parameter [55,56] according to Equations (3) and (4). The selection of the best model was based on RMSE calculation, the mean standardized error (MSE), and the root mean square standardized error (RMSEE) according to Equations (5) and (6).

The Gaussian function was defined as:

$$(h) = \begin{cases} C_0 + C\left(1 - exp\left(\frac{-h^2}{a^2}\right)\right), h > 0 \\ 0, h = 0 \end{cases} \quad (3)$$

The spherical function was defined as:

$$(h) = \begin{cases} C_0 + C\left(\frac{3h}{2a} - \frac{1}{2} - \left(\frac{h}{a}\right)^3\right), 0 < h \leq a \\ C_0 + C, h > a \\ 0, h = 0 \end{cases} \quad (4)$$

where a = the actual ranges for the spherical and circular, h = the spatial lag, C_0 = is the nugget, and C = the partial sill.

$$\text{MSE} = \frac{1}{N}\sum_{i=1}^{N}[Z_1(X_1) - Z_2(X_2)] \quad (5)$$

$$\text{RMSSE} = \sqrt{\frac{1}{N}\sum_{I=1}^{N}[Z_1(x_i) - Z_2(x_i)]^2} \quad (6)$$

2.6. Modelling of SFC in the Study Area

Soil fertility condition (SFC) characterizes the soil nutrient content, i.e., available N, P, K, SOM, and pH (Figure 8), developed using the MLR model. The factors that were selected in this study for calculating fertility status were based on the criteria for crop growth requirements according to [37]. The SFC are used as an indicator for the degree of crop suitability for exact uses [6]. GIS spatial modeling was used for evaluating SFCs based on the following Equation (7).

$$SFC = S * [N * P * K * SOM * pH]^{1/5} \quad (7)$$

where S = score of each parameter.

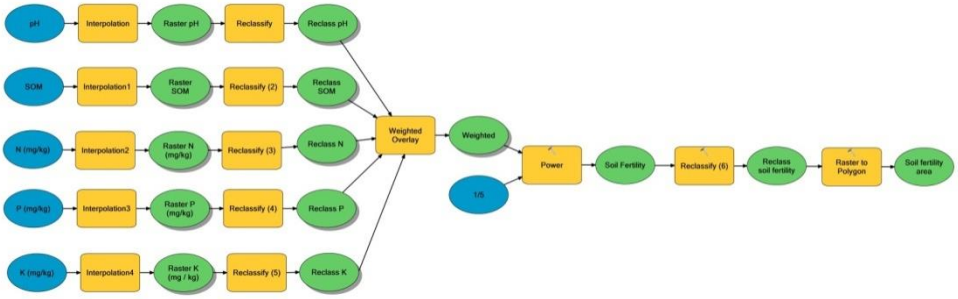

Figure 8. Flow chart devised in this study to model SFC.

The model builder function in Arc GIS 10.7 was used to create the spatial model of SFCs. Selected spatial analysis of the parameters is displayed in a diagram chain [57] (Figure 8). Output from each process is considered as the input for the next process [58]. The subsequent stages were applied in this research to obtain the final SFC map of the investigated area: (a) Interpolation of soil properties to raster layer, with the results from this stage (b) reclassified into five classes (Very low, low, moderate, high, and very high), then (c) scoring each SFC parameter based on Table 2, (d) feeding Equation (7) utilizing the raster calculator tool and finally (f) the outputs from (d) were weighted and overlayed to obtain and display the final SFC map.

Table 2. Score factors of SFC parameters.

Selected Factor	Measuring Unit	1	0.8	0.5	0.2
N	ppm	>80	80–40	40–20	>20
P	ppm	>15	15–10	10–5	<5
K	ppm	>400	400–200	200–100	<100
SOM	%	>2	2–1	1–0.5	<0.5
pH	-	5.5–7	7–7.8	7.9–8.5	>8.5

3. Results and Discussion

3.1. Soil Properties

The results reveal that the values of pH varied from 7.10 to 8.98 within the study area, with an average pH of 7.92. The high value of pH is due to the presence of limestone parent material [6]. These calcareous soils occupy wide areas of Egypt's Western Desert and North Africa [59]. These values of pH indicate a high similarity within the study area (STD = 0.47) [60]. Soil nutrient availability and enzyme and soil organism activity in different kinds of soils are both influenced by values of pH; thus, pH is considered one of the most important factors soil factors [61]. The study area contains a low content of soil organic matter (SOM), ranging from 0.03 to 0.83%. The low values of SOM are logical for arid regions as high temperatures encourage the decomposition of organic matter [60]. For the spatial distribution of SOM %, the highest values were located in the wadi area unit due to the presence of seasonal crops [46]; however, there is a low variation of SOM content with STD ≅ 0.5. Generally, the

Egyptian soils suffer from a deficiency of macronutrients, i.e., N, P, and K have ranges of 3.32 to 87.11, 0.8 to 7.34, and 20.13 to 200.40 ppm, respectively. Concerning SD, the variation in N and K is very wide (STD = 13.04 and 32.27, respectively), with a STD value of1.77 for P. The study area has the climatic and topographic conditions of the northern coast, which is characterized by low values of N, P, and K except for some areas that cultivate seasonal crops. These results are in line with those of [62] (Table 3 and Figure 9).

Table 3. Statistics of measured SFC parameters.

Statistics	M. pH	M. SOM	M. N	M. P	M. K
MAX	8.98	0.83	87.11	7.34	200.40
Mean	7.92	0.38	45.47	4.18	83.37
MIN	7.10	0.03	3.32	0.80	20.13
STD	0.47	0.21	13.04	1.77	32.27

Note: M = measure.

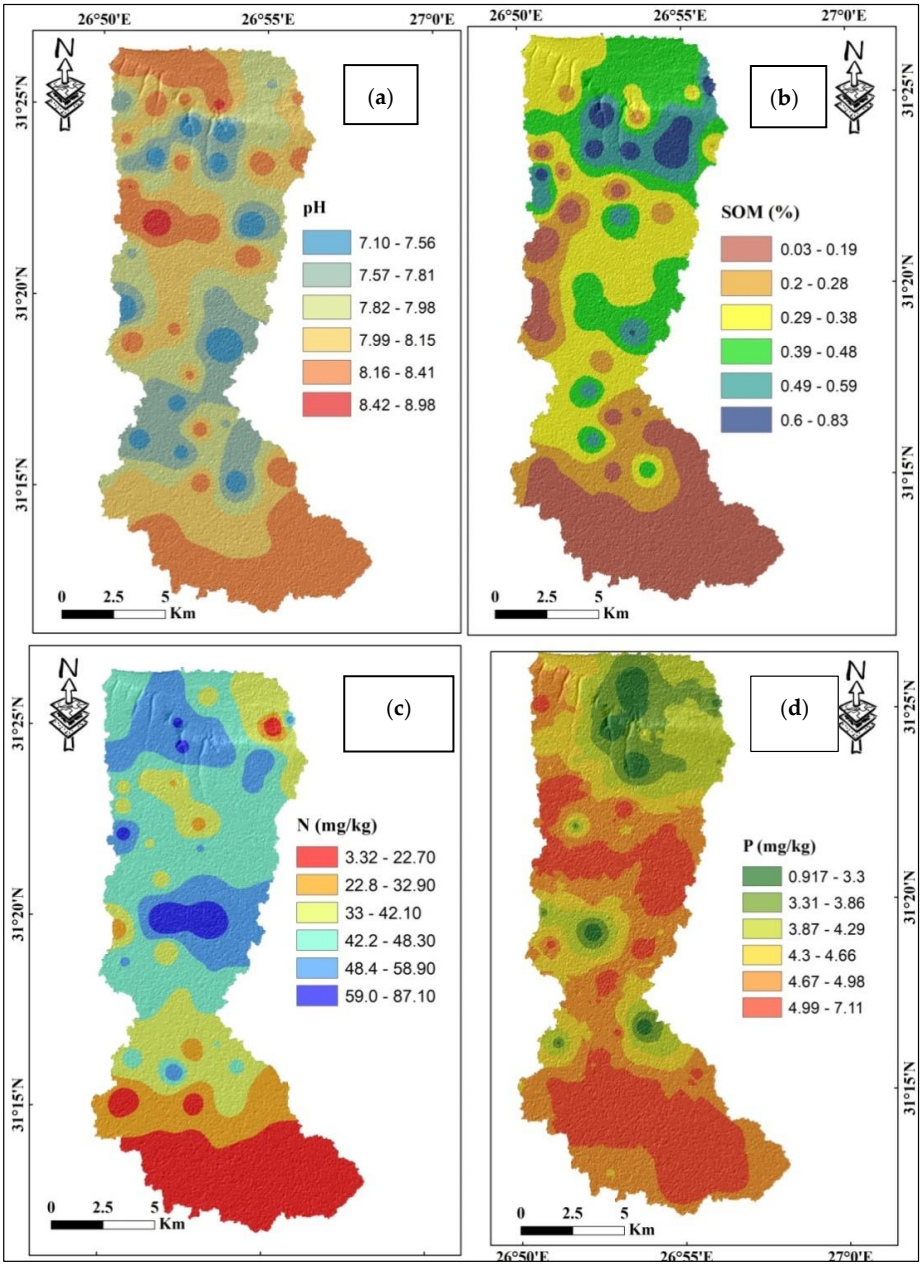

Figure 9. *Cont.*

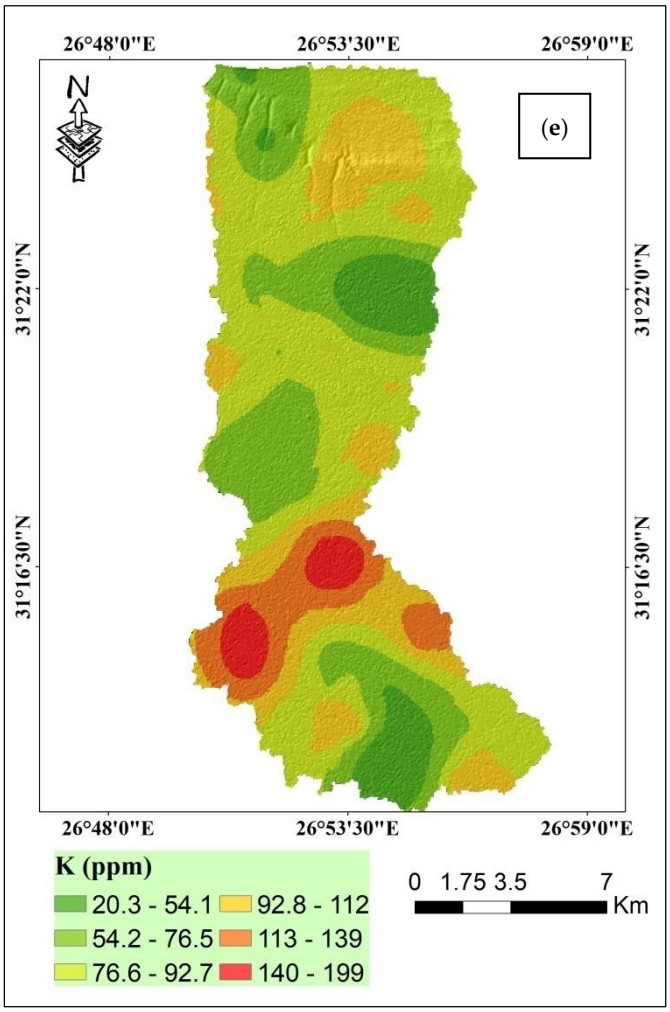

Figure 9. Spatial distribution of measured SOC parameters: (**a**) pH, (**b**) soil organic matter %, (**c**) nitrogen content (ppm), (**d**) phosphorus content (ppm), and (**e**) potassium content (ppm).

3.2. Producing SFC Parameter Using S2A Image

S2A data may help to characterize a given soil gradient, even if only a few soil samples were used during differentiated crop operations (within the process of a precision agriculture) [30]. The following five Equations (8)–(12), were used to obtain the values of pH, SOM %, N, P, and K from the reflectance of the satellite image. OK was then used for the spatial distribution of these selected parameters. An assessment of accuracy was performed by calculating NRMSE (Table 4).

$$\text{pH} = (\text{band } 2 * 3.66) + (\text{band } 3 * 9.744) + (\text{b4} * -0.016) + 4.52 \quad (8)$$

$$\text{SOM \%} = (\text{band } 6 * -0.5567) + (\text{band } 7 * 36.58) + (\text{band } 11 * 0.2359) - 13.43 \quad (9)$$

$$\text{N} = (\text{band } 4 * -78.98) + (\text{band } 5 * 2272.91) - 740.16 \quad (10)$$

$$\text{P} = (\text{band } 6 * -5.76) + (\text{band } 10 * 1089.051) - 1.18 \quad (11)$$

$$\text{K} = (\text{band } 1 * 12{,}930.48) + (\text{band } 2 * -64.75) + (\text{band } 10 * -1107.29) - 468.28 \quad (12)$$

All the studied parameters indicated acceptable results due to R^2 values of 0.75 ± 0.31, 0.82 ± 0.11, 0.74 ± 8.70, 0.50 ± 1.53, and 0.97 ± 7.89 for pH, SOM %, N, P, and K, respectively. NRMSE values were 0.16, 0.14, 0.1, 0.01, and 0.04, respectively (Table 3 and Figure 4). The outputs from our results indicate that MLR is effective for predicting soil properties, with these outputs being consistent with [6,63,64]. The accuracy values (R^2 calibration) were

0.6, 0.7, 0.55, 0.6, and 0.92 for pH, SOM, N, P, and K, respectively. As a whole, spectral reflections are affected by a variety of soil properties and their concentrations [65,66]. Although the determination of respondent parts of a wavelength to dynamic changes in element concentration is very complex, statistical analysis can resolve this issue [6]. The qualitative analysis (visual comparison) and quantitative statistics should be utilized for the assessment of model performance [67], and the results of this research are in line with those of other studies [6,46]. The performance of the model for all selected elements was assessed using determination (adj R). All models showed good fitting with adj R ranging from 0.55 (N) to 0.92 (K).

Table 4. Model validation of soil property values obtained from S2A image.

Selected Parameters	R^2 Calibration	Adjusted R	RMSE	NRMSE	R^2 Validation
pH	0.6	0.54	0.31	0.16	0.75
SOM %	0.7	0.65	0.11	0.14	0.82
N (ppm)	0.55	0.52	8.70	0.1	0.74
P (ppm)	0.6	0.60	1.53	0.01	0.50
K (ppm)	0.92	0.91	7.89	0.04	0.97

3.3. Spatial Distribution of Predicted SOC Parameters Based on OK

The SOC parameter mapping relied on those values which were predicted by applying the above models (Equations (8)–(12)) from the satellite image for each characteristic. OK was utilized for mapping the SOC parameters and the efficacy and ability were measured by calculating RMSE, MSE, and RMSSE, as shown in Table 4. The spatial distribution of pH, and SOM regarding N, P, and K is shown in Figure 9. The predicted pH values ranged from 7.28 to 8.54 in central and northern parts of the study area, whereas the study area was characterized by a low content of SOM with the highest values located in wadi areas due to agricultural activities. The predicated values of N, P, and K ranged from 20.31–66.15, 2.01–6.84, and 24.13–174.59, respectively (Table 5). It can be concluded from these results that the selected soil properties perform as acceptable indicators for soil fertility condition of the study area, with these findings falling in line with those of [6]. The outputs showed that the Gaussian model is fit for SOM, N, and P, whereas the spherical and stable models are suitable for pH and K. It can be concluded from Table 6 that OK has the ability to map selected SOC parameters with high accuracy as RMSEE values are close to 1.00, i.e., 1.01, 0.98, 0.94, 0.95, and 1.00 for pH, SOM, N, P, and K, respectively; these results are consistent with [46,68]. These findings confirm that OK was suitable and reliable for predicting the spatial distribution of selected parameters (Figure 10).

Table 5. Statistics of predicted SFC parameters based on the S2A image.

Statistics	Pred. pH	Pred. SOM	Pred. N	Pred. P	Pred. K
MAX	8.54	0.71	66.15	6.84	174.59
Mean	7.90	0.38	45.47	4.18	83.37
MIN	7.28	0.05	20.31	2.01	24.13
SD	0.35	0.17	9.63	1.40	30.64

Table 6. Geostatistical OK analysis of predicted soil properties (pH, OM, N, P, and K).

Soil Parameters	Transformation	Trend Type	Model Type	Mean	RMSE	MSE	RMSSE	ASE
Pred. pH	Box cox	Constant	Spherical	0	0.34	0	1.01	0.3
Pred. SOM	None	Constant	Gaussian	0	0.16	0.02	0.98	0.2
Pred. N	log	None	Gaussian	5.32	14.1	0.15	0.94	28
Pred. P	log	None	Gaussian	0.01	1.24	0.02	0.95	1.4
Pred. K	Normal score	None	Stable	0.78	26.7	0.03	1.03	25

Note: Pred. = predicted.

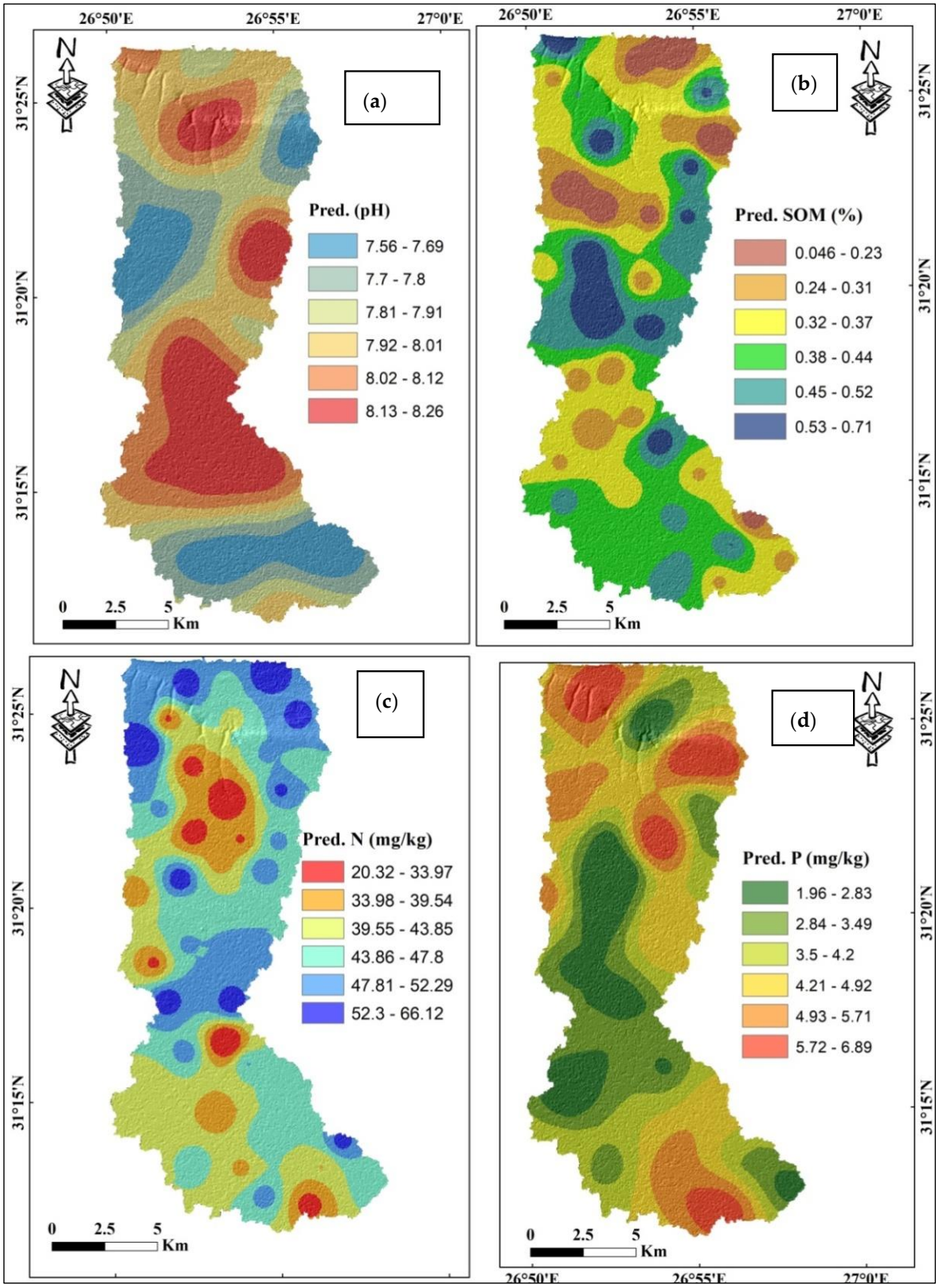

Figure 10. *Cont.*

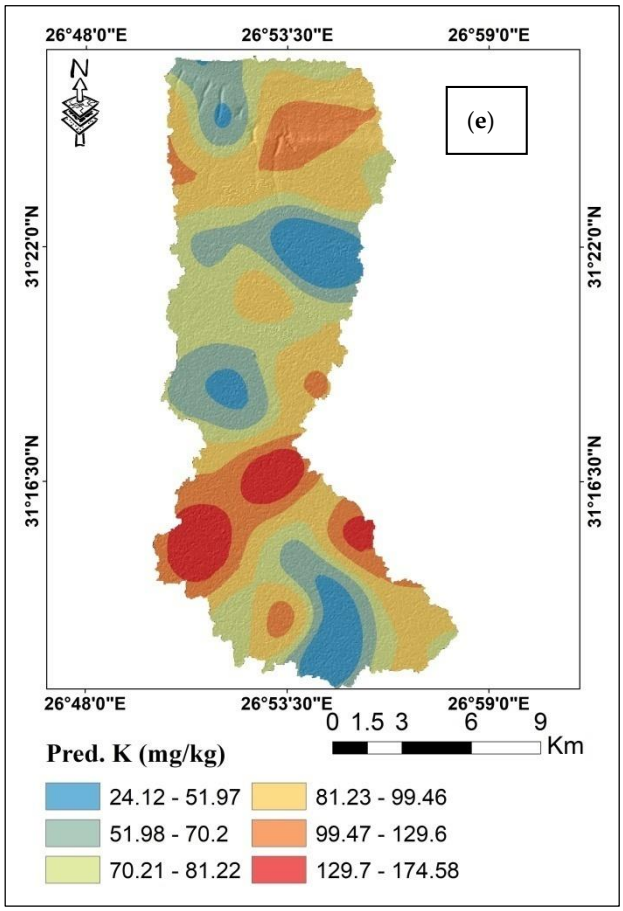

Figure 10. Spatial distribution of predicted SOC parameters: (**a**) pH, (**b**) soil organic matter %, (**c**) nitrogen content (ppm), (**d**) phosphorus content (ppm), and (**e**) potassium content (ppm).

3.4. Multivariate Statistical Analysis (MSA)

A correlation coefficient was used to measure the relationship between the variables and their strength [69,70]. This plays a very important role in dimensionality reduction of sample data and missing value estimations [71]. A Pearson correlation analysis illustrated the correlation between measured and predicted (pred.) soil parameters. There is a significant positive correlation between the pH and pred. pH, where r = 0.75. Furthermore, there is a significant positive correlation between the SOM and pred. SOM (r = 0.8). There is also a significant positive correlation between N and pred. N (r = 0.7), P and pred P (0.5), and K and pred. K (r = 0.92), as seen in Table 7 and Figure 11.

Table 7. Spearman correlations between original and predicated soil properties.

	pH	Pred. pH	OM	Pred. OM	N	Pred. N	P	Pred. P	K	Pred. K
pH	1.00	0.753 **	0.039	−0.124	0.035	0.086	−0.033	−0.051	0.081	0.027
Pred. pH		1.00	0.230	0.111	−0.027	0.081	−0.199	−0.242	0.029	−0.045
OM			1.00	0.791 **	0.311 *	0.177	−0.203	−0.257	−0.033	0.040
Pred. OM				1.00	0.211	0.129	−0.217	−0.084	−0.174	−0.036
N					1.000	0.678 **	−0.057	−0.096	−0.047	0.062
Pred. N						1.000	−0.031	0.006	−0.055	0.070
P							1.000	0.456**	−0.271	−0.165
Pred. P								1.000	−0.223	−0.275
K									1.000	0.925 **
Pred. K										1.00

** *p* values = 0.01 and * = 0.05 level.

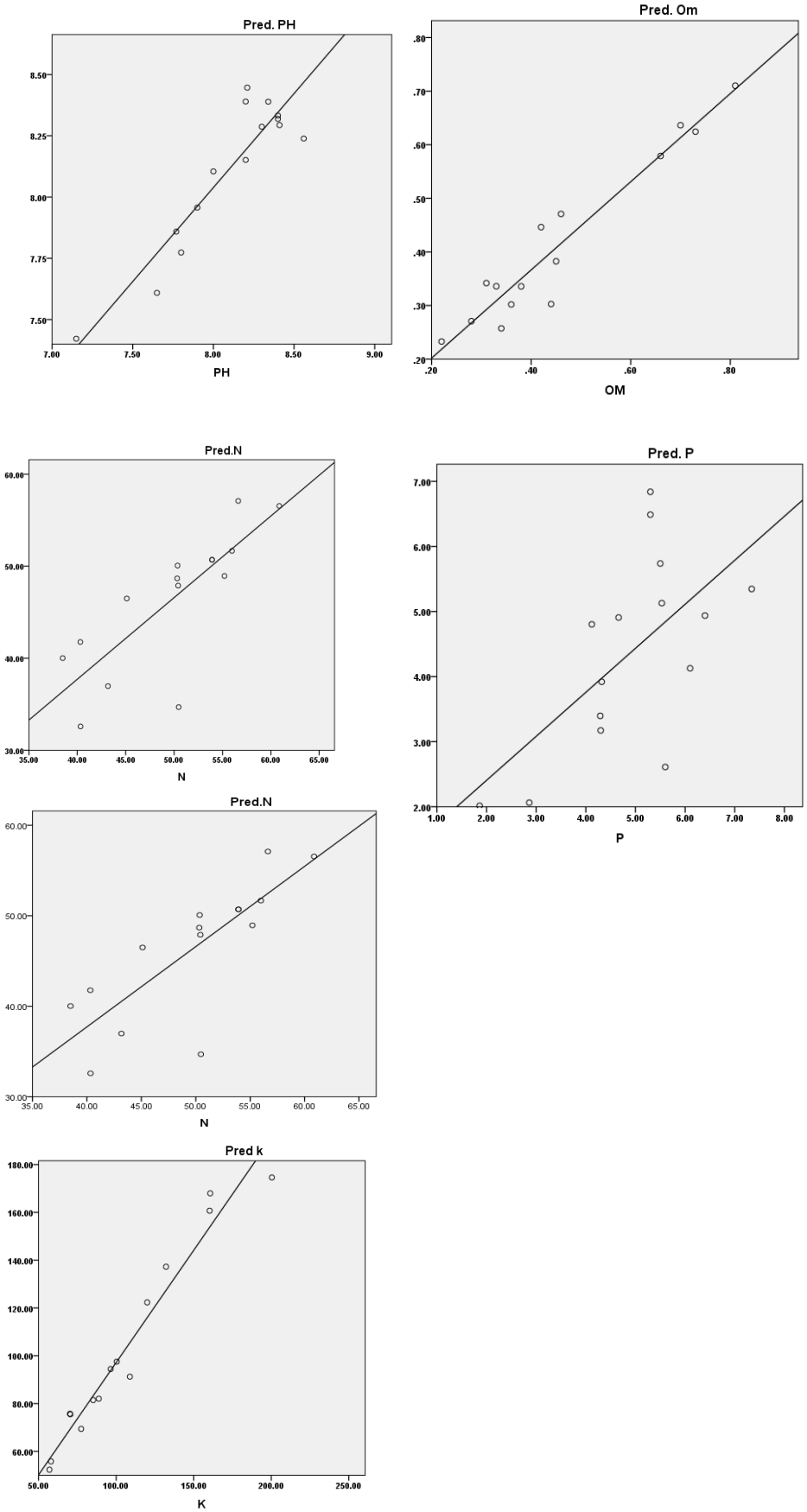

Figure 11. Linear correlation between measured and predicted parameters.

3.5. The SFC of Study Area

The mapping of soil fertility plays an important role in the realization of many applications within relevant research fields, ranging from soil management for sustainability to precision farming concepts [6]. The spatial distribution of SFCs in the study area was produced based on selected pH, SOM, N, P, and K parameters. The study area was classified according to the following three classes: moderate, low, and very low, with areas of 4607.90, 14,900.21, and 705.73 ha, respectively. References terms covered an area of 1155.91 ha (Tables 8 and S1, and Figure 12). The low values of SFCs in the study area are due to the mismanagement of agricultural activities and the location of the study area within an arid zone. Moderate values were noticed in those areas which have agricultural activates and deep profiles with a flat or almost flat surface [71,72]. These results demonstrate that the desert areas of Egypt suffer from a poverty of soil fertility in comparison to the Nile Delta [63,65,73,74] and need suitable management to choose the best crops according to soil quality, water availability, and the climate of an area.

Table 8. Areas of SFC classes in the study area.

SFC Classes	Symbol	Area (Hectare)
Moderate	F3	4607.90
Low	F4	14,900.21
Very low	F5	705.73
References terms	-	1155.91

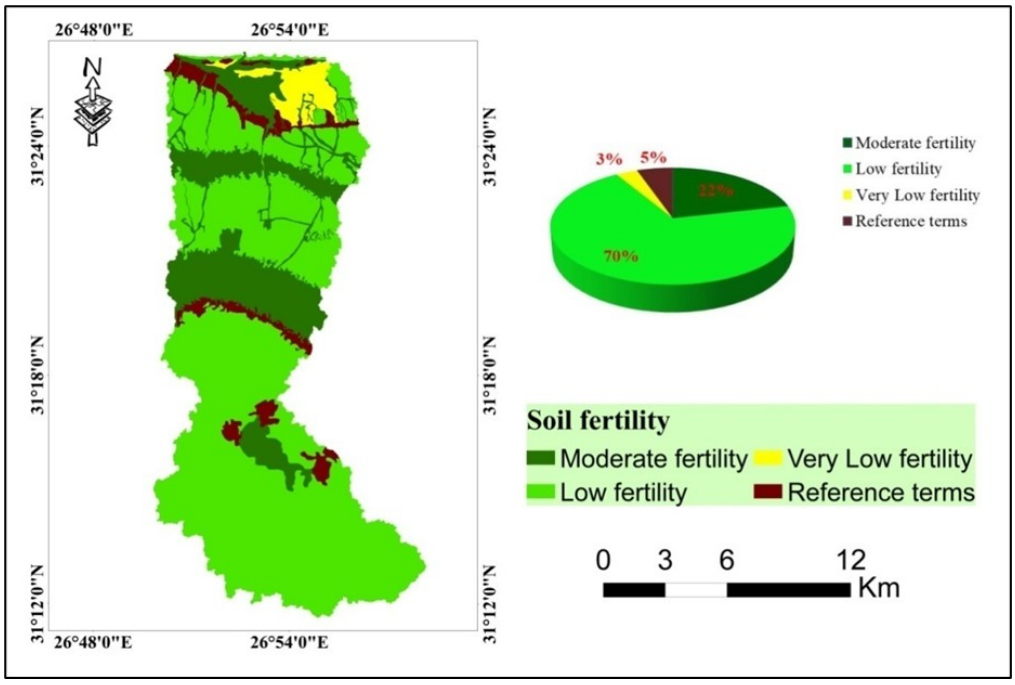

Figure 12. SFC areas of the study area.

4. Conclusions

Reflectance analysis from S2A imagery is a very effective procedure for predicting the pH, SOM, and presence of macro elements (N, P and K) in drylands. The current work aimed to find a relationship between reflectance from S2A imagery and SFC parameter concentrations. MLR was applied as representative of a dryland area to predict soil fertility parameters, with the mapping of those parameters, using ordinary kriging geostatistical analysis, then performed. The results revealed that reflectance within S2A imagery could predict different element concentrations, evidenced by the R2 values of 0.75 ± 0.31, 0.82 ± 0.11, 0.74 ± 8.70, 0.50 ± 1.53, and 0.97 ± 7.89 for pH, SOM %, N, P, and

K, respectively, and NRMSE values of 0.16, 0.14, 0.1, 0.01, and 0.04 also respective to this. The study area was divided into four classes of fertility condition, i.e., low fertility (70%), moderate fertility (22%), very low fertility (3%), and references terms (5%). The procedure herein provides an accurate and low-cost tool for wide implementation in assisting with food security by monitoring soil fertility status in drylands and improving soil conservation. Overcoming dry land ecological and poverty issues is considered one of the most important goals of the global 2030 Agenda for Sustainable Development (SDGs).

Supplementary Materials: The following supporting information can be downloaded at: https://www.mdpi.com/article/10.3390/ijgi11060353/s1, Figure S1: Samples distribution by conditional Latin hypercube (cLHS); Figure S2: Hydrological and metamorphic parameters extracted from R software; Table S1: Weight of final SFC based on GIS model builder.

Author Contributions: Conceptualization Mohamed S. Shokr and Mostafa A. Abdellatif; methodology Mohamed S. Shokr and Mostafa A. Abdellatif; software Mohamed S. Shokr and Mostafa A. Abdellatif; validation, Mohamed S. Shokr and Mostafa A. Abdellatif; formal analysis, Ahmed M. Saleh, Mohamed S. Shokr, Yasser S. A. Mazrouand Mostafa A. Abdellatif; investigation, Mohamed S. Shokr and Mostafa A. Abdellatif; resources Mohamed S. Shokr and Mostafa A. Abdellatif; data curation, Mohamed S. Shokr and Mostafa A. Abdellatif, writing—Mohamed S. Shokr and Ahmed A. El Baroudy, writing—review and editing, Ahmed M. Saleh, Mohamed S. Shokr, Ahmed A. El Baroudy, Esawy K. Mahmoud and Zheli Ding; visualization, Mohamed S. Shokr, Ahmed A. El Baroudyand Zheli Ding; supervision Ahmed M. Saleh, Abdelaziz A. Belal and Esawy K. Mahmoud; project administration Abdelaziz A. Belal; funding acquisition, Yasser S. A. Mazrou and Zheli Ding. All authors have read and agreed to the published version of the manuscript.

Funding: King Khalid University for funding this work, through the Program of Research Groups under grant number (RGP 2/67/43).

Institutional Review Board Statement: Not applicable.

Informed Consent Statement: Not applicable.

Data Availability Statement: Not applicable.

Acknowledgments: The authors extend their appreciation to the Deanship of Scientific Research at King Khalid University for funding this work through the Program of Research Groups under grant number (RGP2/67/43). The authors are grateful to the Senior Foreign Expert Project of China (Grant number G2021034008L).The authors would like to thank the National Authority for Remote Sensing and Space Science (NARSS) for supporting the field survey and remote sensing work.

Conflicts of Interest: The authors declare no conflict of interest.

References

1. Mohamed, E.S.; Abu-Hashim, M.; Belal, A.A.A. Sustainable Indicators in Arid Region: Case Study–Egypt. In *Sustainability of Agricultural Environment in Egypt Soil-Water-Food Nexus, The Handbook of Environmental Chemistry*; Springer Science and Business Media LLC: Berlin/Heidelberg, Germany, 2018; pp. 273–293.
2. AbdelRahman, M.A.; Shalaby, A.; Mohamed, E.S. Comparison of two soil quality indices using two methods based on geographic information system. *Egypt J. Remote Sens. Space Sci.* **2019**, *22*, 127–136. [CrossRef]
3. Abu-hashim, M.; Elsayed, M.; Belal, A.E. Effect of land-use changes and site variables on surface soil organic carbon pool at Mediterranean Region. *J. Afr. Earth Sci.* **2016**, *114*, 78–84. [CrossRef]
4. Hendawy, E.; Belal, A.A.; Mohamed, E.S.; Elfadaly, A.; Murgante, B.; Aldosari, A.A.; Lasaponara, R. The prediction and assessment of the impacts of soil sealing on agricultural land in the North Nile Delta (Egypt) using satellite data and GIS modeling. *Sustainability* **2019**, *11*, 4662. [CrossRef]
5. Vaudour, E.; Gomez, Y.C.; Fouad, P. Lagacherie, Sentinel-2 image capacities to predict common topsoil properties of temperate and Mediterranean agroecosystems. *Remote Sens. Environ.* **2019**, *223*, 21–33, ISSN 0034-4257. [CrossRef]
6. Mohamed, E.S.; Baroudy, A.A.E.; El-beshbeshy, T.; Emam, M.; Belal, A.A.; Elfadaly, A.; Aldosari, A.A.; Ali, A.M.; Lasaponara, R. Vis-NIR Spectroscopy and Satellite Landsat-8 OLI Data to Map Soil Nutrients in Arid Conditions: A Case Study of the Northwest Coast of Egypt. *Remote Sens.* **2020**, *12*, 3716. [CrossRef]
7. Horta, A.; Malone, B.; Stockmann, U.; Minasny, B.; Bishop, T.F.A.; McBratney, A.B.; Pallasser, R.; Pozza, L. Potential of integrated field spectroscopy and spatial analysis for enhanced assessment of soil contamination: A prospective review. *Geoderma* **2015**, *241*, 180–209. [CrossRef]

8. Angelopoulou, T.; Tziolas, N.; Balafoutis, A.; Zalidis, G.; Bochtis, D. Remote sensing techniques for soil organic carbon estimation: A review. *Remote Sens.* **2019**, *11*, 676. [CrossRef]
9. Minasny, B.; McBratney, A.B. A conditioned Latin hypercube method for sampling in the presence of ancillary information. *Comput. Geosci.* **2006**, *32*, 1378–1388. [CrossRef]
10. Brungard, C.W.; Boettinger, J.L. Conditioned Latin hypercube sampling: Optimal sample size for digital soil mapping of arid Rangelands in Utah, USA. In *Digital Soil Mapping*; Boettinger, J.L., Howell, D.W., Moore, A.C., Hartemink, A.E., Kienast-Brown, S., Eds.; Progress in Soil Science; Springer: Dordrecht, The Netherlands, 2010.
11. Brungard, C.W.; Boettinger, J.L.; Duniway, M.C.; Wills, S.A.; Edwards, T.C., Jr. Machine learning for predicting soil classes in three semi-arid landscapes. *Geoderma* **2015**, *239–240*, 68–83. [CrossRef]
12. Worsham, L.; Markewitz, D.; Nibbelink, N.P.; West, L.T. A comparison of three field sampling methods to estimate soil carbon content. *Forest Sci.* **2012**, *58*, 513–522. [CrossRef]
13. Taghizadeh-Mehrjardi, R.; Nabiollahi, K.; Minasny, B.; Triantafilis, J. Comparing data mining classifiers to predict spatial distribution of USDA-family soil groups in Baneh region, Iran. *Geoderma* **2015**, *253–254*, 67–77. [CrossRef]
14. Levi, M.R.; Rasmussen, C. Covariate selection with iterative principal component analysis for predicting physical soil properties. *Geoderma* **2014**, *219*, 46–57. [CrossRef]
15. Taghizadeh-Mehrjardi, R.; Minasny, B.; Sarmadian, F.; Malone, B.P. Digital mappingof soil salinity in Ardakan region, central Iran. *Geoderma* **2014**, *213*, 15–28. [CrossRef]
16. Lacoste, D.; Gaspard, P. Isometric fluctuation relations for equilibrium states with broken symmetry. *Phys. Rev. Lett.* **2014**, *113*, 24. [CrossRef]
17. Scarpone, C.; Schmidt, M.G.; Bulmer, C.E.; Knudby, A. Modelling soil thickness in the critical zone for Southern British Columbia. *Geoderma* **2016**, *282*, 59–69. [CrossRef]
18. Waruru, B.K.; Shepherd, K.D.; Ndegwa, G.M.; Sila, A.M. Estimation of wet aggregation: Indices using soil properties and diffuse reflectance near infrared spectroscopy, an application of classification and regression tree analysis. *Biosyst. Eng.* **2016**, *152*, 148–164. [CrossRef]
19. Adhikari, K.; Hartemink, A.E. Soil organic carbon increases under intensive agriculture in the Central Sands, Wisconsin, USA. *Geoderma Reg.* **2017**, *10*, 115–125. [CrossRef]
20. Domenech, M.B.; Castro-Franco, M.; Costa, J.L.; Amiotti, N.M. Sampling scheme optimization to map soil depth to petrocalcic horizon at field scale. *Geoderma* **2017**, *290*, 75–82. [CrossRef]
21. Jeong, G.; Oeverdieck, H.; Park, S.J.; Huwe, B.; Ließ, M. Spatial soil nutrients prediction using three supervised learning methods for assessment of land potentials in complex terrain. *Catena* **2017**, *154*, 73–84. [CrossRef]
22. Babaei, F.; Zolfaghari, A.A.; Yazdani, M.R.; Sadeghipour, A. Spatial analysis of infiltration in agricultural lands in arid areas of Iran. *CATENA* **2018**, *170*, 25–35. [CrossRef]
23. Nawar, S.; Buddenbaum, H.; Hill, J.; Kozak, J. Modeling and mapping of soil salinity with reflectance spectroscopy and landsat data using two quantitative methods (PLSR and MARS). *Remote Sens.* **2014**, *6*, 10813–10834. [CrossRef]
24. Selige, T.; Bohner, J.; Schmidhalter, U. High resolution topsoil mapping using hyper spectral image and field data in multivariate regression modeling procedures. *Geoderma* **2006**, *136*, 235–244. [CrossRef]
25. Stevens, A.; Udelhoeven, T.; Denis, A.; Tychon, B.; Lioy, R.; Hoffman, L.; Van Wesemael, B. Measuring soil organic carbon in croplands at regional scale using airborne imaging spectroscopy. *Geoderma* **2010**, *158*, 32–45. [CrossRef]
26. Gomaes, C.; Coulouma, G.; Lagacherie, P. Regional Predictions of eight common soil properties and their spatial structures from hyperspectral Vis-NIR data. *Geoderma* **2012**, *189–190*, 176–185.
27. Gomaes, C.; Lagacherie, P.; Bacha, S. Using an VNIR/SWIR hyperspectral image to map topsoil properties over bare soil surfaces in the Cap Bon region (Tunsia). In *Digital Soil Assessment and Beyond*; Minsny, B., Malone, B.P., McBratney, A.B., Eds.; Springer: Berlin/Heidelberg, Germany, 2012; pp. 387–392.
28. Vaudour, E.; Gilliot, J.M.; Bel, L.; Lefevre, J.; Chehdi, K. Regional prediction of soil organic carbon content over temperature croplands using visible near-infrared airborne hyperspectral imagery and synchronous field spectra. *Int. J. Appl. Earth Obs. Geoinf.* **2016**, *49*, 24–38.
29. Baroudy, A.A.E.; Ali, A.M.; Mohamed, E.S.; Moghanm, F.S.; Shokr, M.S.; Savin, I.; Poddubsky, A.; Ding, Z.; Kheir, A.M.S.; Aldosari, A.A.; et al. Modeling Land Suitability for Rice Crop Using Remote Sensing and Soil Quality Indicators: The Case Study of the Nile Delta. *Sustainability* **2020**, *12*, 9653. [CrossRef]
30. Santaga, F.S.; Agnelli, A.; Leccese, A.; Vizzari, M. Using Sentinel-2 for Simplifying Soil Sampling and Mapping: Two Case Studies in Umbria, Italy. *Remote Sens.* **2021**, *13*, 3379. [CrossRef]
31. Ben-Dor, E.; Banin, A. Near-Infrared Analysis as a Rapid Method to Simultaneously Evaluate Several Soil Properties 94. *Soil Sci. Soc. Am. J.* **1995**, *59*, 364–372. [CrossRef]
32. Adeline, K.; Gomez, C.; Gorretta, N.; Roger, J.M. predictive ability of soil properties to spectral degradation from laboratory Vis-NIR spectroscopy data. *Geoderma* **2017**, *288*, 143–153. [CrossRef]
33. Gomez, C.; Adeline, K.; Bacha, S.; Driessn, B.; Gorretta, N.; Lagacherie, P.; Roger, J.M.; Briottet, X. Sensitivity of clay content prediction to spectral configuration of VNIR/SWIR imaging data. *Geoderma* **2015**, *288*, 143–153.
34. Rossel, R.V.; McBratney, A.B. Laboratory evaluation of a proximal sensing technique for simultaneous measurement of soil clay and water content. *Geoderma* **1998**, *85*, 19–39. [CrossRef]

35. Abd-Elmabod, S.K.; Muñoz-Rojas, M.; Jordán, A.; Anaya-Romero, M.; Phillips, J.D.; Jones, L.; Zhang, Z.; Pereira, P.; Fleskens, L.; Van Der Ploeg, M. Climate change impacts on agricultural suitability and yield reduction in a Mediterranean region. *Geoderma* **2020**, *374*, 114453. [CrossRef]
36. Shokr, M.S.; El Baroudy, A.A.E.; Fullen, M.A.; El-Beshbeshy, T.R.; Ali, R.R.; Elhalim, A.; Guerra, A.J.T.; Jorge, M.C.O. Mapping of heavy metal contamination In alluvial soils of the Middle Nile Delta of Egypt. *J. Environ. Eng. Landsc. Manag.* **2016**, *24*, 218–231. [CrossRef]
37. El Baroudy, A.A. Mapping and evaluating land suitability using a GIS-based model. *Catena* **2016**, *140*, 96–104. [CrossRef]
38. Barbosa, A.; Marinho, T.; Martin, N.; Hovakimyan, N. Multi-Stream CNN for spatial resource allocation: A crop management application. In Proceedings of the IEEE/CVF Conference on Computer Vision and Pattern Recognition Workshops, Seattle, WA, USA, 14–19 June 2020; pp. 58–59.
39. Preston, W.; Araújo do Nascimento, C.W.; Agra Bezerra da Silva, Y.J.; Silva, D.J.; Alves Ferreira, H. Soil fertility changes in vineyards of a semiarid region in Brazil. *J. Soil Sci. Plant Nutr.* **2017**, *17*, 672–685. [CrossRef]
40. Shrivastava, P.; Kumar, R. Soil salinity. A serious environmental issue and plant growth promoting bacteria as one of the tools for its alleviation. *Saudi J. Biol. Sci.* **2015**, *22*, 123–131. [CrossRef] [PubMed]
41. Schütz, L.; Gattinger, A.; Meier, M.; Müller, A.; Boller, T.; Mäder, P.; Mathimaran, N. Improving crop yield and nutrient use efficiency via biofertilization—A global meta-analysis. *Front. Plant Sci.* **2018**, *8*, 2204. [CrossRef]
42. Khdery, G.; Gad, A.A.; El-Zeiny, A.M. Spectroscopic Characterization of Plant Cover in El-Fayoum Governorate, Egypt. *Egypt J. Soil Sci.* **2020**, *60*, 397–408. [CrossRef]
43. Abd-Elmabod, S.K.; Jordán, A.; Fleskens, L.; Phillips, J.D.; Muñoz-Rojas, M.; Van der Ploeg, M.; Anaya- Romero, M.; De la Rosa, D. Modelling agricultural suitability along soil transects under current conditions and improved scenario of soil factors. In *Soil Mapping and Process Modeling for Sustainable Land Use Management*; Elsevier: Amsterdam, The Netherland, 2017; pp. 193–219, ISBN 9780128052006.
44. Khalifa, M.E.; Beshay, N.F. Soil classification and potentiality assessment for some rainfed areas at West of Matrouh, Northwestern Coast of Egypt. *Alex. Sci. Exch. J. Int. Q.J. Sci. Agric. Environ.* **2015**, *36*, 325–341.
45. Ministry of Industry and Mineral Resources (MIMR). *The Egyptian Geological Survey and Mining Authority Scale 1:2:000.000*; Ministry of Industry and Mineral Resources: Riyadh, Saudi Arabia, 1981.
46. Abdellatif, M.A.; El Baroudy, A.A.; Arshad, M.; Mahmoud, E.K.; Saleh, A.M.; Moghanm, F.S.; Shaltout, K.H.; Eid, E.M.; Shokr, M.S. A GIS-Based Approach for the Quantitative Assessment of Soil Quality and Sustainable Agriculture. *Sustainability* **2021**, *13*, 13438. [CrossRef]
47. Soil Survey Staff (USDA). Soil Survey Staff (USDA). Soil survey field and laboratory methods manual. In *Soil Survey Investigations Report No. 51*; Version 2.0; Department of Agriculture, Natural Resources Conservation Service: Washington, DC, USA, 2014.
48. Roudier, P. Clhs: A R Package for Conditioned Latin Hypercube Sampling. 2011. Available online: http://cran.rproject.org/web/packages/clhs/index.html (accessed on 14 October 2021).
49. Fidalgo, E.C.C.; Pedreira, B.C.C.G.; Abreu, M.B.; Moura, I.B.; Godoy, M.D.P. *Uso e Cobertura da Terra naBaciaHidrográfica do Rio Guapi-Macacu*; (Documentos 105); Embrapa Solos: Rio de Janeiro, Brazil, 2008.
50. Rukun, L. *Analysis Methods of Soil Agricultural Chemistry*; Agriculutural Science and Technology Press: Beijing, China, 1999.
51. Yang, Y.; Zhu, J.; Tong, X.; Wang, D. The Spatial Pattern Characteristics of Soil Nutrients at the Field Scale. In *Proceedings of the Computer and Computing Technologies in Agriculture II, Volume 1. CCTA 2008. IFIP Advances in Information and Communication Technology*; Li, D., Zhao, C., Eds.; Springer: Boston, MA, USA, 2009; Volume 293. [CrossRef]
52. Bui, Q.-T.; Jamet, C.; Vantrepotte, V.; Mériaux, X.; Cauvin, A.; Mograne, M.A. Evaluation of Sentinel-2/MSI Atmospheric Correction Algorithms over Two Contrasted French Coastal Waters. *Remote Sens.* **2022**, *14*, 1099. [CrossRef]
53. Dangal, S.R.; Sanderman, J.; Wills, S.; Ramirez-Lopez, L. Accurate and Precise Prediction of Soil Properties from a Large Mid-Infrared Spectral Library. *Soil Syst.* **2019**, *3*, 11. [CrossRef]
54. Mohamed, E.; Belal, A.A.; Ali, R.R.; Saleh, A.; Hendawy, E.A. Land degradation. In *The Soils of Egypt*; Springer Cham: Basel, Switzerland, 2019; pp. 159–174.
55. Otto, S.A.; Kadin, M.; Casini, M.; Torres, M.A.; Blenckner, T. A quantitative framework for selecting and validating food web indicators. *Ecol. Indic.* **2018**, *84*, 619–631. [CrossRef]
56. Biswas, A.; Si, B.C. Model averaging for semivariogram model parameters. Adv. *Agrophys. Res.* **2013**, *4*, 81–96.
57. Shokr, M.S.; Abdellatif, M.A.; El Baroudy, A.A.; Elnashar, A.; Ali, E.F.; Belal, A.A.; Attia, W.; Ahmed, M.; Aldosari, A.A.; Szantoi, Z.; et al. Development of A Spatial Model for Soil Quality Assessment under Arid and Semi-Arid Conditions. *Sustainability* **2021**, *13*, 2893. [CrossRef]
58. El Behairy, R.A.; El Baroudy, A.A.; Ibrahim, M.M.; Kheir, A.M.; Shokr, M.S. Modelling and Assessment of Irrigation Water Quality Index Using GIS in Semi-arid Region for Sustainable Agriculture. *Water Air Soil Pollut.* **2021**, *232*, 352. [CrossRef]
59. El-Aziz, S.H.A. Evaluation of land suitability for main irrigated crops in the North-Western Region of Libya. *Eurasian J. Soil Sci.* **2018**, *7*, 73–86. [CrossRef]
60. Ali, R.R.; Moghanm, F.S. Variation of soil properties over the landforms around Idku lake, Egypt. *Egypt J. Remote Sens. Space Sci.* **2013**, *16*, 91–101. [CrossRef]

61. Ostovari, Y.; Ghorbani-Dashtaki, S.; Bahrami, H.A.; Abbasi, M.; Dematte, J.A.M.; Arthur, E.; Panagos, P. Towards prediction of soil erodibility, SOM and $CaCO_3$ using laboratory Vis-NIR spectra: A case study in a semi-arid region of Iran. *Geoderma* **2018**, *314*, 102–112. [CrossRef]
62. Belal, A.A.; Mohamed, E.S.; Abu-hashim, M.S.D. Land Evaluation Based on GIS-Spatial Multi-Criteria Evaluation (SMCE) for Agricultural Development in Dry Wadi, Eastern Desert. *Egypt Int. J. Soil Sci.* **2015**, *10*, 100–116. [CrossRef]
63. Mohamed, E.S. Spatial assessment of desertification in north Sinai using modified MEDLAUS model. *Arab. J. Geosci.* **2013**, *6*, 4647–4659. [CrossRef]
64. Mohamed, E.S.; Ali, A.; El-Shirbeny, M.; Abutaleb, K.; Shaddad, S.M. Mapping soil moisture and their correlation with crop pattern using remotely sensed data in arid region. *Egypt. J. Remote Sens. Space Sci.* **2019**, *23*, 347–353. [CrossRef]
65. Mohamed, E.; Abdellatif, M.; Abd-Elmabod, S.K.; Khalil, M. Estimation of surface runoff using NRCS curve number in some areas in northwest coast, Egypt. In Proceedings of the E3S Web of Conferences, Barcelona, Spain, 10–12 February 2020; EDP Sciences: Les Ulis, France; Volume 167, p. 2002.
66. Zhang, Z.; Yu, D.; Shi, X.; Warner, E.; Ren, H.; Sun, W.; Tan, M.; Wang, H. Application of categorical information in the spatial prediction of soil organic carbon in the red soil area of China. *Soil Sci.* **2010**, *56*, 307–318. [CrossRef]
67. Moriasi, D.N.; Arnold, J.G.; Van Liew, M.W.; Bingner, R.L.; Harmel, R.D.; Veith, T.L. Model evaluation guidelines for systematic quantification of accuracy in watershed simulations. *ASABE* **2007**, *50*, 885–900. [CrossRef]
68. Aldabaa, A.; Yousif, I.A.H. Geostatistical approach for land suitability assessment of some desert soils. *Egypt. J. Soil Sci.* **2020**, *60*, 195–205. [CrossRef]
69. Gao, L.; Zhu, X.; Han, Z.; Wang, L.; Zhao, G.; Jiang, Y. Spectroscopy-Based Soil Organic Matter Estimation in Brown Forest Soil Areas of the Shandong Peninsula, China. *Pedosphere* **2019**, *29*, 810–818. [CrossRef]
70. Fu, C.; Tian, A.; Zhu, D.; Zhao, J.; Xiong, H. Estimation of Salinity Content in Different Saline-Alkali Zones Based on Machine Learning Model Using FOD Pretreatment Method. *Remote Sens.* **2021**, *13*, 5140. [CrossRef]
71. Abdel-Kader, F.H. Digital soil mapping at pilot sites in the northwest coast of Egypt: A multinomial logistic regression approach. *Egypt J. Remote Sens. Space Sci.* **2011**, *14*, 29–40. [CrossRef]
72. Said, M.E.S.; Ali, A.M.; Borin, M.; Abd-Elmabod, S.K.; Aldosari, A.A.; Khalil, M.M.N.; Abdel-Fattah, M.K. On the Use of Multivariate Analysis and Land Evaluation for Potential Agricultural Development of the Northwestern Coast of Egypt. *Agronomy* **2020**, *10*, 1318. [CrossRef]
73. Barseem, M.S.; el Sayed, A.N.; Youssef, A.M. Impact of geologic setting on the groundwater occurrence in wadis El Sanab, Hashem, and Khrega using geoelectrical methods northwestern coast. *Egypt Arab J. Geosci.* **2014**, *7*, 5127–5139. [CrossRef]
74. Abdel-Fattah, M.K.; Abd-Elmabod, S.K.; Aldosari, A.A.; Elrys, A.S.; Mohamed, E.S. Multivariate Analysis for Assessing Irrigation Water Quality. A Case Study of the Bahr Mouise Canal, Eastern Nile Delta. *Water* **2020**, *12*, 2537. [CrossRef]